ISSN 1070-3632, Russian Journal of General Chemistry, 2007, Vol. 77, No. 4, pp. 721–739. © Pleiades Publishing, Ltd., 2007.
Original Russian Text © V.I. Isaeva, L.M. Kustov, 2007, published in Russkii Khimicheskii Zhurnal, 2007, Vol. 50, No. 6, pp. 56–72.

# Metal–Organic Frameworks—New Materials for Hydrogen Storage

**V. I. Isaeva and L. M. Kustov**

*Zelinskii Institute of Organic Chemistry, Russian Academy of Sciences,*
*Leninskii pr. 47, Moscow, 119991 Russia*
*tel.: (495)137-2935*
*fax: (495)135-5328*
*e-mail: LMK@ioc.ac.ru, sharf@ioc.ac.ru*

Received September 26, 2006

**Abstract**—Published data on the physical sorption of hydrogen by new materials with a large specific surface area, crystalline microporous metal–organic frameworks (MOFs), are systematized and analyzed. The hydrogen-accumulating properties of MOFs are compared with those of traditional materials (charcoals and zeolites) and nanocarbon systems. The role of secondary hydrogen spillover in the development of new approaches to increase the adsorption capacity of hydrogen storage materials is separately considered.
**DOI:** 10.1134/S1070363207040342

Over the past 10–15 years the interest in hydrogen as motor fuel has mounted up [1]. Hydrogen can be burnt in internal combustion engines or oxidized in fuel cells. According to calculations, fuel cells are almost double as efficient as internal combustion engines. At present the technologies of hydrogen fuel cells and internal combustion engines and methods of hydrogen production are better developed than methods of hydrogen storage, and an indispensable condition for the progress of hydrogen energetics is search for new hydrogen storage systems.

The target parameters declared by the US Department of Energy (DOE) for hydrogen storage systems are known: to reach by 2010 hydrogen capacities of no less than 6.0 wt% at a storage density of 45 kg $H_2\,m^{-3}$ (in other sources, 6.5 wt% and 62 kg $H_2\,m^{-3}$ [2]. By 2015, a capacity of 9.0 wt% and a density of 81 kg $m^{-3}$ are targeted, which meets real requirements of motor industry. Hydrogen is presently stored in a number of ways: in high-pressure gas cylinders (up to 80 MPa); in cryogenic tanks at 21 K; in the adsorbed state in materials with a high specific surface area at temperatures below 100 K; and in a chemically bound state at atmospheric pressure in intermetallic, covalent, or ionic compounds [3].

## PHYSICAL SORPTION OF HYDROGEN

The weight density of liquid hydrogen is as little as 70.8 kg $m^{-3}$ at 20 K and atmospheric pressure, and 5 kg of $H_2$ occupy, under standard conditions, a fairly large volume ~56 $m^3$ [3]. Hydrogen storage systems based on physical sorption characteristically have high volumetric and gravimetric densities at low working pressures [4], and they are fairly cheap and structurally simple. However, their essential drawbacks are low hydrogen capacity, from 1 to to ~4.5 wt% and sorption temperature, 273 K and below, usually it is the liquid nitrogen temperature.

Ideally, an adsorbent should have a high hydrogen capacity at room temperature and ability for fast hydrogen adsorption and desorption. For such parameters the $H_2$–adsorbent interaction energy should be about 5 kJ $mol^{-1}$ [5]. The general problem of the physical sorption of hydrogen by various systems with a high specific surface area (metal–organic frameworks, zeolites, and carbon materials) consists in that the energy of hydrogen binding with surface is too low to provide satisfactory sorption of this gas at temperatures above the liquid nitrogen temperature. As the physical sorption occurs due to weak van der Waals interaction between the adsorbate and adsorbent, saturation can only be attained at low temperatures, and hydrogen capacities are low even is the adsorbent has a high specific surface area [3]. The search for effective hydrogen sorbents should largely be focused on systems with stronger surface–hydrogen interactions [6].

In the present review we have analyzed published data on the physical sorption of hydrogen by new materials with a high specific surface area, viz. crystalline microporous metal–organic frameworks (MOFs). This class of compounds includes coordina-

**Table 1.** Hydrogen adsorption on carbon nanomaterials

| Material [a] | Formal surface area (BET), $m^2 g^{-1}$ | $H_2$ adsorption, wt % | Adsorption conditions | Reference |
|---|---|---|---|---|
| CNF | – | 0.7 | 20°C, 10 MPa | [4] |
| CNF + liquid crystals | 1758 | 3.5 | 77.3 K, 0.8 MPa | [15] |
| SWNTs | 2560 | 4.5 | 77 K, 0.1 MPa | [16] |
| | The same | 0.5 | 25°C, 0.1 MPa | |
| MWNTs | – | 2.27 | 77 K, 10.3 MPa | [2] |
| | – | ≤0.3 | 25°C, 10.61 MPa | |

[a] Here and hereinafter: (CNF) Carbon nanofiber, (SWNTs) single-wall nanotubes, (AX-21) supeactivated charcoal, and (MWNTs) multiwall nanonanotubes.

tion polymers comprising metal ions bridged by organic ligands. An attempt has been made compare the hydrogen-accumulating properties of MOFs with those of traditional materials (charcoals and zeolites) and nanocarbon systems.

Separate attention has been given to the role of secondary hydrogen spillover in the development of new ways to increasing the adsorption capacity of hydrogen storage materials.

## HIGH-POROSITY CARBON CARRIERS

At present various carbon carriers for reversible hydrogen sorption [4, 7–11] are known. The advantages of carbon carriers for hydrogen storage are a developed surface, low density compared to intermetallides, chemical inertness, and tolerance to cooling [10]. As potential hydrogen sorbents, systems with various specific surface areas and pore sizes, both traditional (charcoals and graphites), and new (porous carbon strings, nanocarbone fibers and tubes) [4, 12] were explored. These materials feature fast kinetics and full reversibility of hydrogen adsorption, which implies a physical interaction [3]. However, graphite has a very low hydrogen capacity at room temperature, on account of strong interaction between graphene (cylindrical fullerene formed by 6-membered rings) flakes and, as a consequence, hindered hydrogen diffusion between them.

*Carbon nanofibers.* The most accessible carbon structure, charcoal with a high specific surface area possesses a hydrogen capacity of up to 5–6 wt% (77 K, 3.5 MPa). An essential disadvantage of this system is a low sorption temperature (cryogenic conditions) [13]. Numerous attempts were undertaken to develop new carbon materials for hydrogen storage at higher temperatures and atmospheric pressure. Carbon nanofibers (CNFs) that represent layered graphite nanostructures were suggested as such materials [4, 7, 11, 14]. However, the presently available hydrogen capacity of these structures at room temperature is as low as 0.7 wt%, and, therewith, a high pressure (about 10 MPa) is required (Table 1) [4].

To increase the hydrogen capacity of CNFs, they are preliminary treated and modified. Thus, exposure to water vapor much increases the BET specific surface area of carbon fibers from 116 to 1758 $m^2 g^{-1}$. The hydrogen sorption capacity of CNFs can be increased to 3.5 wt%, which corresponds to a 60% hydrogen surface coverage (77.3 K, 0.65 MPa [15]). In the latter example, the increased hydrogen capacity of the modified CNF sample is associated with its increased specific surface area. However, with nanofibers, unlike charcoals and carbon nanotubes, no linear dependence between hydrogen sorption capacity and specific surface area is observed [4]. This is probably connected with the fact that CNFs contain narrow pores inaccessible for nitrogen in specific surface measurements but accessible for hydrogen. The hydrogen capacity of nanofibers implicitly correlates with their structure, since CNFs and charcoals with the same specific surface areas have different sorption characteristics.

The physical meaning of high BET specific surface areas of microporous systems will be considered below in more detail.

*Carbon nanotubes.* Now carbon nanotubes (CNTs)—systems with a high density of micropores, representing convolute graphene sheets [4, 7, 17]—are considered the most promising carbon materials for hydrogen storage applications. The principal difference between carbon nanotubes and a high-surface-area graphite consists in the curvature of graphene sheets and presence of cavities inside tubes. Different adsorption capacities of exterior and interior nanotube

**Table 2.** Hydrogen adsorption on zeolites

| Material | Formal surface area (BET), $m^2 g^{-1}$ | $H_2$ adsorption, wt % | Adsorption conditions | Reference |
|---|---|---|---|---|
| ZSM-5 | – | 0.7 | 77 K, 0.1 MPa | [46] |
| NaY | 725 | 1.8 | 77 K, 1.5 MPa | [21] |
| CaX | – | 2.19 | 77 K | [22] |

surfaces have been reported. Exterior walls of carbon nanotubes and other cylindrically-shaped graphite materials are characterized by a weaker π-electron system, and, thereof, lower potential of the surface for physical hydrogen sorption than a flat graphene. On the contrary, interior walls possess a higher potential: The adsorption centers on the interior surface of nanotubes reportedly have a fairly high energy of physical sorption (up to 30 kJ $mol^{-1}$) [10]. Such an increase in the potential energy is explained by the fact that in microporous solid substances with pores whose diameter is commensurate with molecular, the potential fields of opposite walls overlap, thereby enhancing adsorbate attraction compared to a flat surface. It should be noted that tube curvature can affect the potential energy but not the quantity of adsorbed hydrogen [16].

At present single- and multi-wall nanotubes are used for hydrogen adsorption. An essential drawback of carbon materials is that they necessitate cryogenic conditions for physical sorption. The hydrogen capacity of single-wall nanotubes at atmospheric pressure is about 5 wt% at 77 K and <1 wt% at room temperature and high pressure. The respective values for multiwall nanotubes are 2.27 wt% at 77 K and 0.3 wt% at room temperature (Table 1) [2].

Carbon nanotubes are distinguished by morphology and way of preparation, for example, cracking of hydrocarbons over the $Ni/Al_2O_3$ catalyst chemical vapor deposition, or activation [8, 17].

Zuttel [3] theoretically estimated the highest possible quantity of hydrogen physically adsorbed on a CNT with a specific surface area of 1315 $m^2 g^{-1}$ at ~2 wt% at 77 K [3]. However, later Panella and Hirsher [16] experimentally obtained a hydrogen capacity of 4.5 wt% (77 K) for a CNT sample with double the surface area (2560 $m^2 g^{-1}$). It should be noted that the highest possible CNT specific surface area is 2630 $m^2 g^{-1}$, which corresponds to two-side coverage of a graphene sheet. Carbon nanotubes feature a strictly linear correlation between specific surface area and hydrogen adsorption capacity.

According to the opinion of some authors who studied the reversible hydrogen sorption on superactivated charcoals and nanocarbon materials in a wide range of pressures and temperatures, the real hydrogen capacity at room temperature and pressures of up to 3.5 MPa is lower than 0.1 wt% for all types nanocarbon materials [7, 18]. Analysis of an abundant experimental evidence for pressures of up to 11 MPa and temperatures spanning the range from –80 to 500°C made Tibbets et al. [7] to cast doubt on the ability of the studied systems to adsorb more than 1% of hydrogen at room temperature. This conclusion was made more than 5 years ago and has not yet been ruled out. Thus, the problem of reversible physical hydrogen sorption at room temperature could not yet be solved by means of nanocarbon materials.

## ZEOLITES

By now general laws of physical hydrogen sorption on zeolites of various structures and compositions (A, Rho, X, Y, and also as Ca, K, and Na forms) have been revealed. Experimental conditions have been varied over a wide range of temperatures (77–573 K) and pressures (2.5–10 MPa) [19–22]. It has been shown that the adsorption capacity of zeolites is controlled by two main factors: the structure of framework, specifically accessible free space, and the nature of cations which are hydrogen binding centers. With zeolites, like with most carbon carriers, a linear dependence of the quantity of adsorbed hydrogen on specific surface area is observed.

Investigation of adsorption centers in HY zeolite by means IR and EXAFS spectroscopies showed that faujasite adsorbs hydrogen at 20 K inside super-cages, giving rise to 1 : 1 $–OH\cdots H_2$ complexes with the Brønsted acid groups of the zeolites. Less specific interactions with cage walls were also revealed. In the case of the sodalite structure, small cages with hexagonal "apertures" are scarcely accessible for hydrogen because of the high potential barrier [23]. This is probably connected with the fact that both cations have very close energies of hydrogen bonding. Thus the highest gravimetric capacity (Table 2) is characteristic of CaX: 2.19 wt% at 77 K. The hydrogen sorption of NaY ($S_{sp}$ 725 $m^2 g^{-1}$) is slightly lower:

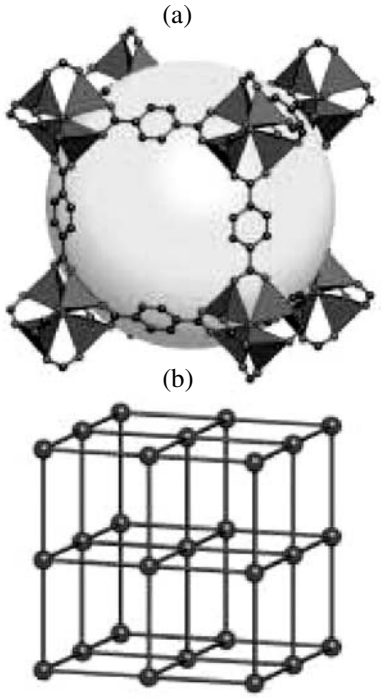


**Fig. 1.** Structure and topology of MOF-5: (a) model showing the cubic framework and shapes of small and large pores; (b) topology of MOF-5 as a spherical rod model.

1.8 wt% (77 K, 1.5 MPa) [21]. Introduction in the cage of $Ca^{2+}$ ions increases the gravimetric hydrogen capacity, since its content in zeolite is half those of singly charged $Na^+$ and $K^+$. Apparently, the hydrogen capacity of zeolites is fairly difficult to further increase in this way because of the limited possibility of introducing extra-framework cations serving as additional centers of hydrogen binding. This possibility, in its turn, is determined by the structure of the zeolite. For example, in A and Rho zeolites, pore blocking with extra-framework cations is the principal obstacle for hydrogen adsorption. It should be noted that X and Y zeolites lack such blocking [23].

The adsorption capacity of zeolites can probably be increased by introducing metals with a high energy of hydrogen binding, such as Pd(0). In this case, hydrogen is adsorbed in the atomic state to form a metal hydride phase, and, as shown by H/D isotopic substitution experiments, even small sodalite cages become therewith accessible for hydrogen [23]. The ways to increasing the hydrogen capacity of some sorbents due to the spillover effect are considered below.

## CRYSTAL MICROPOROUS METAL–ORGANIC POLYMERS

AT present there exist a number of overlapping and mutually complementary definitions for hybride structures possessing a low density, high porosity and crystallinity, and large specific surface area (from 500 to 4500 $m^2 g^{-1}$): crystalline microporous metal–organic coordination polymers, metal–organic coordination lattices, metal–organic frameworks, and organic analogs of zeolites. In what follows to define these systems we will use a commonly accepted abbreviation MOFs (metal-organic frameworks). According to Yaghi et al. [24], who synthesized a series of MOFs with controlled pore size, the term "metal–organic framework" is the most appropriate, since it nicely reflects the ordered and predictable structure of these materials.

Metal–organic frameworks re[resent a new class of microporous polymeric materials whose structure-forming units are mononuclear or polynuclear coordination centers: metal ions linked together by organic fragments [25, 26]. Speaking about preparation of MOFs, researchers often use such terms as "design," "combinatorial" or "logic synthesis," "molecular design," or "modular chemistry." These definitions are underlain by the fact that their synthesis is a realization of an attractive but not infrequently hardly practical idea of constructing new materials with controllable physical and chemical properties from molecular building blocks.

*Structure of MOFs.* The structure MOFs can be presented as a lattice construction in which rigid organic fragments link, like rods, inorganic clusters locating in the nodes of the lattice. Figure 1 shows various ways of depicting the MOF-5 structure (the labels of individual MOFs comprise figures relating to their synthesis time). In Fig. 1a, the structure of MOF-5 is represented in the form of $ZnO_4$ tetrahedra linked by phenylene dicarboxylate units to form a cubic framework with 8-Å small pores and a large spherical pore 12(15) Å in diameter, inscribed in a cube. The diameter of the large pore is determined by the distance between the van der Waals surfaces of framework atoms. In Fig. 1b, the MOF-5 topology (primitive cubic lattice) is represented as a spherical rod model.

The size and chemical nature of the frame of the free space of cages formed due to such a frame architecture, is determined by the length and functionality of organic linkers [24]. By varying initial molecular building blocks and their arrangement one can control the architecture of the material and its proper-

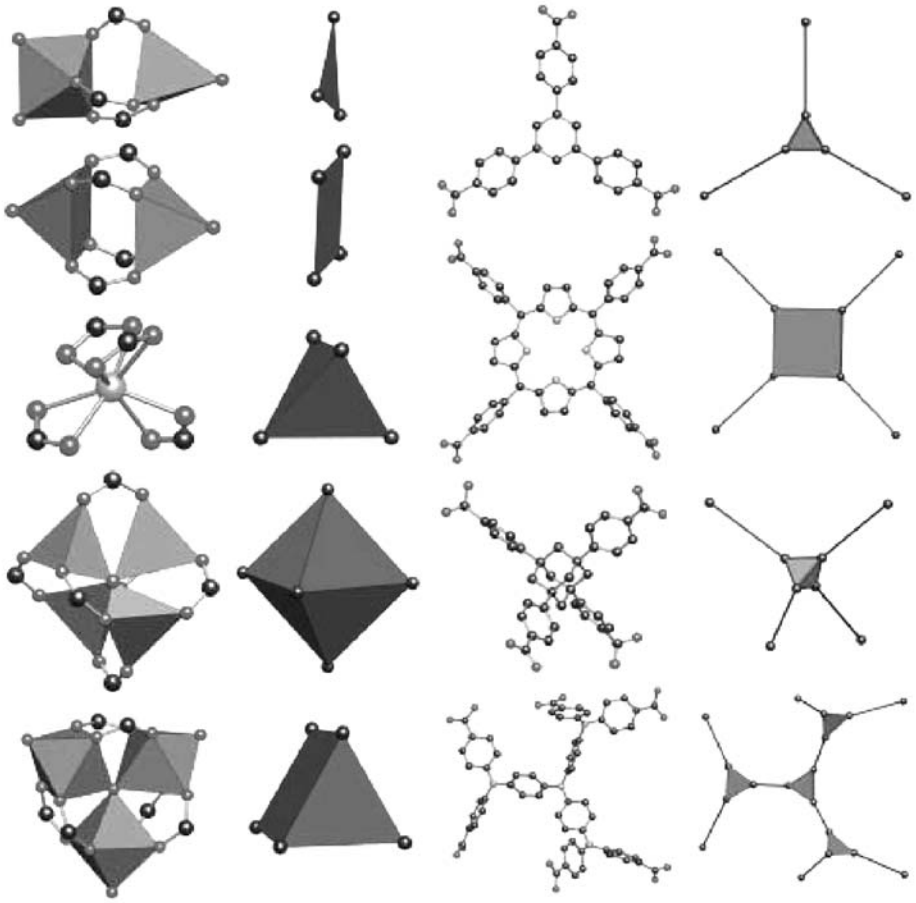

**Fig. 2.** Example secondary structural units in carboxylate MOFs.

ties. Yaghi and co-workers [27] introduced the concept "reticular synthesis" which radically differs from organic retrosynthesis in that the structural integrity and rigidity of building blocks are preserved during the entire lattice assembly process. Reticular synthesis is also quite different from supramolecular assembly, since the resulting metal–organic framework has all building blocks linked by strong covalent bonds. Thus, the synthesis of MOFs demands not only appropriate choice of necessary building blocks (modules), but also prediction of the resulting structure. For clearer understanding of the structure of the framework being constructed, the term "secondary building unit" (SBU) was introduced, which was originally related to basic fragments of zeolites [24]. When applied to MOFs, secondary units represent simple geometric figures reflecting the structure of inorganic clusters or coordination spheres of metal ions, that are arranged in a certain framework by means of organic linkers. Examples of SBUs in carboxylate MOFs are given in Fig. 2. Such approach clearly determines the steric structure of the resulting framework and allows use of a great number of inorganic and organic SBUs of various geometries. The task of a researcher consists in determining reaction conditions ensuring in situ formation of an inorganic SBU of specific configuration. Combination of an inorganic structural unit with rigid organic provides a metal–organic lattice of preset structure [28].

The above approach is illustrated by the synthesis of isoreticular three-dimensional porous MOFs (IRMOFs) with a common formula and the same lattice topology (Fig. 3) [29]. These frameworks are constructed of rigid organic fragments (prototyped by completely deprotonated 1,4-phenylenedicarboxylic acid) and $Zn^{2+}$ ions. The structure comprises oxo-centered $Zn_4O$ tetrahedra located in cube corners and linked by six carboxylate bridges to form octahedral SBUs. The size of pores was varied by means of various-length carboxylate units containing biphenyl, tetrahydropyrene, pyrene, and terphenyl fragments [Scheme (1)]. Furthermore, a series of IRMOFs with functional groups, such as –Br, $–NH_2$, $–C_2H_4–$,

**Scheme 1.**

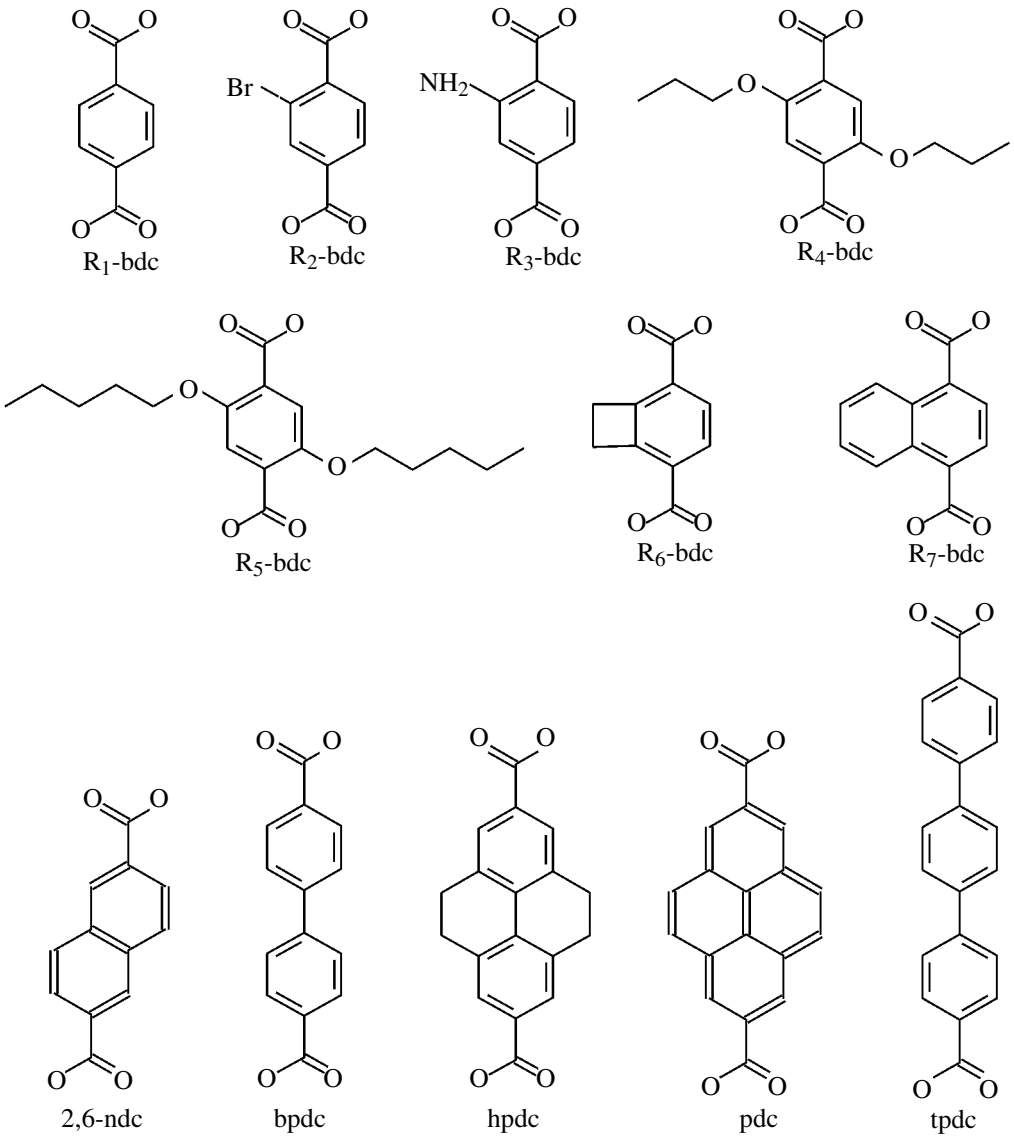


Organic fragments of isoreticular MOFs.

$-C_4H_6-$, $-OC_3H_7$, and $-OC_5H_{11}-$, as organic linkers has been synthesized.

Over the past years about 11000 of MOFs [25, 26, 28, 30] have been obtained. Of them about 3000 compounds are three-dimensional and about 6000 are two-dimensional. The organic linkers in MOFs can be divided into 2 basic types: charged and uncharged. The most important charged and uncharged linkers are carboxylate ions and heterocyclic ligands, respectively. The most frequently used metal ions are Cu(II), Mn(II), Zn(II), Ni(II), and lanthanide ions.

Flexible heterocyclic fragmens, as well as aliphatic linkers that allow for free rotation about their axis are disadvantageous in the spacial indefiniteness of the ligand surrounding of the metal ion. As a consequence, the architecture of the resulting framework is difficult to control. By contrast, rigid aromatic polydentate carboxylate linkers possessing chelate-forming properties allow metal ions to be firmly fixed in metal carboxylate lattice nodes or secondary structural blocks, thereby ensuring rigidity of the MOF structure and predetermining the framework topology [27].

Porous MOFs radically differ from traditional porous crystalline materials, such as molecular sieves, in that MOF pores contain no walls. The free interior space of MOFs is formed by linked open channels and

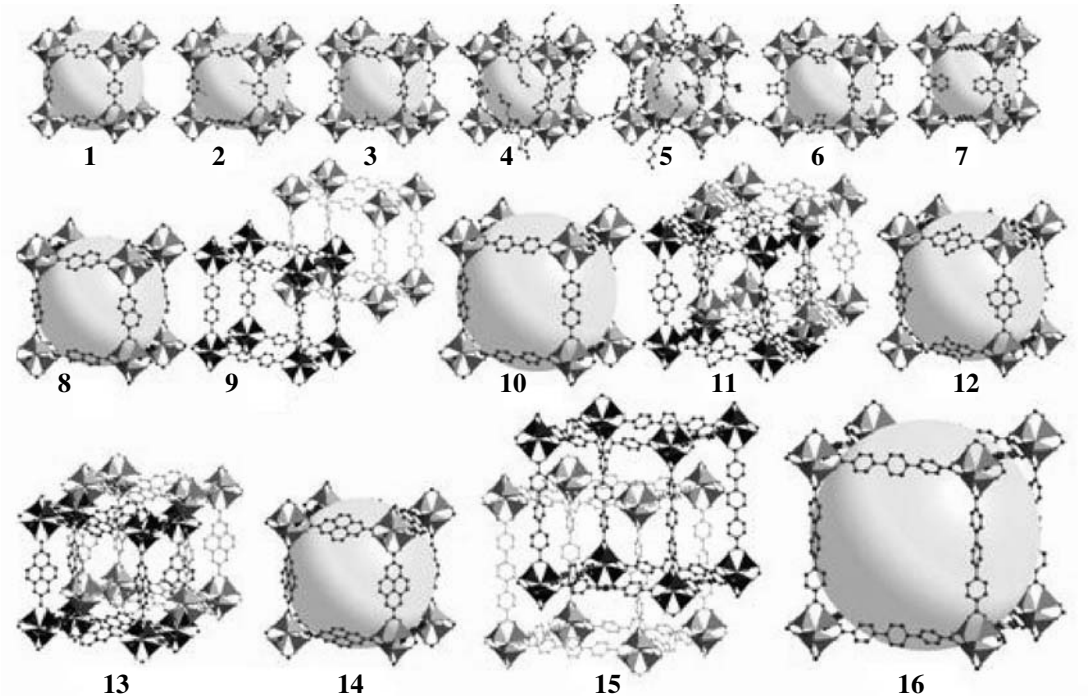


**Fig. 3.** Isoreticular crystal structure of IRMOFs (X-ray diffraction data). The number of structure corresponds to the number of IRMOF.

cavities (less than 2 nm in diameter) in crossing points of these channels, which ensures a high specific surface area and large pores (about double as large as in zeolites). Such cavities become accessible for adsorbate molecules after removal of solvent or reagent molecules trapped during MOF synthesis. The pore volume in a great number of MOFs (0.8–2.5 $cm^3 g^{-1}$) is several times as large as in zeolites (0.3–0.5 $cm^3 g^{-1}$ in A, ZSM-5, and faujasite zeolites). The pore size in MOFs can be controlled by appropriately selecting the organic fragment [31]. For example, all IRMOFs synthesized by Yaghi and co-workers are high-porosity materials with a very low crystal density. The free space inside these lattice structures varies from 55.8% in IRMOF-5 (organic fragment R5-BDC) to 91.1% of the total volume in IRMOF-16 (organic fragment TPDC); therewith, the density varies from 1.0 up to 0.21 $cm^3 g^{-1}$ (for designations of organic fragments, see notes to Tables 3 and 4). These values are rather remarkable, since the free interior space in most open zeolites is no more than 50% of the total volume [27]. An important advantage of MOFs over traditional sorbents is their homogeneous pore-size distribution. The shapes of pores in MOFs are quite diverse [31]. Unlike spherical, elliptic, and slot pores, characteristic for zeolites, MOFs have square, rectangular, and triangular pores [32–35]. Such a diverse pore geometry favors selective sorption.

**Table 3.** Adsorption characteristics of MOFs

| MOF | Formal surface area (BET), $m^2 g^{-1}$ | Pore volume, $cm^3 g^{-1}$ | $H_2$ adsorption, wt% | Conditions, reference |
|---|---|---|---|---|
| $Zn_4O(bdc)_3$ IRMOF-1, MOF-5 | 3362 | 1.19 | 1.32 | 77 K, 0.1 MPa [48] |
| The same | 2630 | 0.93 | 1.0 | 25°C, 2 MPa [51] |
| " | 1466 | 0.52 | 1.65 | 25°C, 4.8 MPa [50] |
| " | 1014 | | 1.6 | 25°C, 1.0 MPa [16] |
| $Zn_4O(Br\text{-}bdc)_3$, IRMOF-2 | 2544, 1722 [a] | 0.88 | 1.2 | 77 K, 0.1 MPa [44] |

**Table 3.** (Contd.)

| MOF[a] | Formal surface area (BET), $m^2 g^{-1}$ | Pore volume, $cm^3 g^{-1}$ | $H_2$ adsorption, wt % | Conditions, reference |
|---|---|---|---|---|
| $Zn_4O(NH_2\text{-bdc})_3$, IRMOF-3 | 3062, 2446[b] | 1.07 | 1.4 | The same |
| $Zn_4O(R_6\text{-bdc})_3$, IRMOF-6 | 3263, 2476[b] | 0.93 | 1.0 | " |
| $Zn_4O(ndc)_3$, IRMOF-8 | 1466 | 0.52 | 1.5 | 77 K, 0.1 MPa [49] |
| $Zn_4O(bpdc)_3$, IRMOF-9 | 2613, 1904[b] | 0.9 | 1.0 | 77 K, 0.1 MPa [44] |
| $Zn_4O(hpdc)_3$, IRMOF-11 | 1911 | 0.68 | 1.62 | 77 K, 0.1 MPa [48] |
| $Zn_4O(pdc)_3$, IRMOF-13 | 2100, 1551[b] | 0.73 | 1.73 | 77 K, 0.1 MPa [44] |
| $Zn_4O(tmbdc)_3$, IRMOF-18 | 1501 | 0.53 | 0.89 | 77 K, 0.1 MPa [48] |
| $Zn_4O(ttdc)_3$, IRMOF-20 | 4346 | 1.53 | 1.31 | 77 K, 0.1 MPa [44] |
| $Zn_4O(btb)_3$, IRMOF-177 | 4526 | 1.61 | 1.25 | 77 K, 0.1 MPa [48] |
| Al(OH)bdc, MIL-53(Al) | 1590, 1020[b] | – | 3.8 | 77 K, 1.6 MPa [47] |
| Cr(OH)bdc, MIL-53(Cr) | 1590, 1020[b] | – | 3.1 | The same |
| Cu(hfipbb) $(H_2hfipbb)_{0.5}$ | | | 1.0 | 25°C, 4.8 MPa [50] |
| $Cu_3(TATB)_2(H_2O)_3$ | 3800 | | 1.9 | 77 K [49] |
| $Mn(HCO_2)_2$ | 240,[b] 297[c] | | 0.9 | 77 K, 0.1 MPa [46] |
| $Zn_2$[1,4-(bdc)2 (dabco)] | 1450 | – | 2.0 | 77 K, 0.1 MPa [52] |
| $Cu_2$(bptc), MOF-505 | 1646 | 0.63 | 2.48 | 77 K, 0.1 MPa [53] |
| $Cu_2(btc)_{4/3}$, HKUST-1 | 2175, 1507[b] | 0.75 | 2.5 | 77 K, 0.1 MPa [44] |
| $Zn_2$[2,5-$(OH)_2$-1,4-$(bdc)_2$] MOF-74 | 1132, 783[b] | 0.39 | 1.7 | The same |
| $[Zn_4(\mu_4\text{-}O)(L_1)_3 \cdot (DMF)_2]$ | 502[d] | 0.20 | 1.12 | 25°C, 4.8 MPa [54] |
| $[Zn_4(\mu_4\text{-}O)(L_2)_3]$ | 396[d] | 0.13 | 0.98 | The same |

[a] (bdc) Phenylene-1,4-dicarboxylate, ($R^6$-bdc) 1,2-dihydrocyclobutylphenylene-3,6-dicarboxylate, (ndc) naphthalenedicarboxylate, (bpdc) biphenyldicarboxylate, (hpdc) 4,5,9,10-tetrahydropyrene-2,7-dicarboxylate, (tmbdc) 2,3,5,6-tetramethylphenylene-1,4-dicarboxylate, (pdc) pyrene-2,7-dicarboxylate, (ttdc) thieno[3,2-*b*]thiophene-2,5-dicarboxylate, (btb) 1,3,5-tris(4-carboxyphenyl)-benzene, ($H_2$hfipbb) 4,4'-(hexafluoroisopropylidene)bisbenzoic acid, (dabco) 1,4-diazabicyclo[2,2,2]octane, (bptc) biphenyltetracarboxylate, (btc) phenylene-1,3,5-tricarboxylate, ($L_1$) 6,6'-dichloro-2,2'-diethoxy-2,2'-1,1'bonaphthyl-4,4'-dibenzoate, ($L_2$) 6,6'-dichloro-2,2'-dibenzyloxy-2,2'-1,1'-binaphthyl-4,4'-dibenzoate, (TATB) 4,4',4''-*S*-triazine2,4,6-triethylbenzoate. [b] By $N_2$ absorption at 77 K. [c] By $CO_2$ adsorption at 195 K. [d] By $CO_2$ adsorption at 273 K.

When referring to MOFs with rigid carboxylate linkers, the term "permanent" porosity is frequently used. This is because, unlike what is observed with MOFs containing heterocyclic ligands, these MOFs are not destroyed after removal from pores of guest molecules [36]. Differently, the "permanent" porosity of MOFs means their stability in a vacuum. The concept of MOF porosity is closely connected with the definition "the open metal–organic framework" which is used for adequate description of materials containing nonbonded mobile solvent molecules in the free space of the framework [24]. The TGA decomposition points of most carboxylate MOFs span the range 300–500°C, and, therefore, such MOFs are stable at temperatures exceeding the desorption temperature of guest molecules [37]. Such thermal

**Table 4.** Geometric characteristics of MOFs

| MOF[a] | Free/fixed pore diameter, Å[b] | Fraction of accessible pore volume[c] | Free volume, % | Reference |
|---|---|---|---|---|
| $Zn_4O(bdc)_3$, IRMOF-1, MOF-5 | 7.8/15.2 | 0.59 | 79.2 | [48] |
| $Zn_4O(Br\text{-}bdc)_3$, IRMOF-2 | 7.5/16.4 | | 78.4 | [44] |
| $Zn_4O(NH_2\text{-}bdc)_3$, IRMOF-3 | 9.6/18.6 | | 78.7 | [44] |
| $Zn_4O(C_3H_7O\text{-}bdc)_3$, IRMOF-4 | 5.4/14.1 | | 64.6 | [29] |
| $Zn_4O(C_3H_7O\text{-}bdc)_3$, IRMOF-5 | 3.6/12.3 | | 55.8 | [29] |
| $Zn_4O(R_6\text{-}bdc)_3$, IRMOF-6 | 5.9/15.2 | 0.50 | 77.5 | [44] |
| $Zn_4O(R_7\text{-}bdc)_3$, IRMOF-7 | 5.5/13.6 | | 76.6 | [29] |
| $Zn_4O(ndc)_3$, IRMOF-8 | 8.4/18.0 | 0.66 | | [49] |
| $Zn_4O(bpdc)_3$, IRMOF-9 | 10.6/14.5 | | 74.7 | [44] |
| $Zn_4O(bpdc)_3$, IRMOF-10 | 15.4/24.5 | | 87.0 | [29] |
| $Zn_4O(hpdc)_3$, IRMOF-11 | 6.0/12.4 | 0.4 | 69.1 | [48] |
| $Zn_4O(hpdc)_3$, IRMOF-12 | 13.0/24.5 | | 84.3 | [29] |
| $Zn_4O(pdc)_3$, IRMOF-13 | 10.2/15.8 | | 70.2 | [44] |
| $Zn_4O(pdc)_3$, IRMOF-14 | 13.8/24.5 | | 85.3 | [29] |
| $Zn_4O(tpdc)_3$, IRMOF-15 | 8.1/12.8 | | 79.8 | [29] |
| $Zn_4O(tpdc)_3$, IRMOF-16 | 19.1/28.8 | | 91.1 | [29] |
| $Zn_4O(tmbdc)_3$, IRMOF-18 | 5.4/13.8 | 0.42 | | [48] |
| $Zn_4O(ttdc)_3$, IRMOF-20 | | | | [44] |
| Zn4O(btb)3, IRMOF-177 | 9.6/11.8 | 0.63 | | [48] |
| Al(OH)bdc, MIL-53(Al) | 6.4/6.4 | 0.29 | | [47] |
| Cr(OH)bdc, MIL-53(Cr) | 6.6/6.6 | 0.29 | | [47] |
| $Cu(hfipbb)(H_2hfipbb)_{0.5}$ | 3.0/4.7 | 0.03 | 11.6 | [50] |
| $Cu_3(TATB)_2(H_2O)_3$ | | | | [49] |
| $Mn(HCO_2)_2$ | 3.0/4.7 | 0.10 | 33.0 | [46] |
| $Zn_2[1,4\text{-}(bdc)_2(dabco)]$ | 7.8/9.5 | 0.45 | | [52] |
| $Cu_2(bptc)$, MOF-505 | 6.7/10.1 | 0.37 | 37.1 | [53] |
| $Cu_2(btc)_{4/3}$, HKUST-1 | | | | [44] |
| $Zn_2[2,5\text{-}(OH)_2\ 1,4\text{-}(bdc)_2]$, MOF-74 | | | | [44] |
| $[Zn_4(\mu_4\text{-}O)(L_1)_3(DMF)_2]$ | 3.8/7.8 | 0.21 | | [54] |
| $[Zn_4(\mu_4\text{-}O)(L_2)_3]$ | 3.8/5.4 | 0.17 | | [54] |

[a] (tpdc) Triphenyldicarboxylate. [b] The free diameter corresponds to the largest sphere capable of entering the small pore of the metal–organic framework. Fixed diameter is the diameter of the largest sphere inscribed into the largest pore of the metal–organic framework. [c] The fraction of free accessible pore volume was calculated from the model radius 1.45 Å which corresponds to the kinetic diameter of hydrogen molecule (2.8 Å).

stability is quite essential for practical application of carboxylate MOFs.

The majority of three-dimensional (3*d*) MOFs feature a high surface area (up to 4500 $m^2\ g^{-1}$), which is an order of magnitude larger than those of zeolites and superactivated charcoals. For example, the theoretical maximum for carbon adsorbents, as already mentioned above, is ~2630 $m^2\ g^{-1}$, which corresponds to two-side coverage of the graphene sheet. It should be noted that specific surface areas measured by the BET procedure for most microporous materials, including MOFs, are formal, on account of micropore volume filling [31]. It is known that the analysis of adsorption data in terms of the BET equation does not allow for micropores, since the adsorbent surface is postulated to be energetically uniform [38]. In micropores, the force fields of neighboring walls overlap,

thus increasing the adsorption potential and, as a consequence, adsorption is carried out not only due to wall coverage of pores but also due to their volume filling. All microporous systems, including MOFs, characteristically show type I isotherms involving a steep ascend at low $P/P_0$ values and a plateau in the field of saturation, and, therewith, in the presence of broad (secondary) micropores, a smoother transition to plateau and its shift to higher $P/P_0$ values are observed. In case of MOFs, we can only speak about a formal specific surface area which allows mutual comparison of microporous systems of the same sort.

*Synthesis of carboxylate MOFs.* Unlike traditional porous carriers and mesoporous materials like MCM, metal–organic frameworks are synthesized in one stage in fairly mild conditions and with high yields (up to 95%). The synthesis is generally performed by precipitation of the product from a solution of the starting reagents. The process of MOF formation is similar to the synthesis of an organic polymer. Therefore, it is important that the rate of formation of the insoluble product is high enough to avoid recrystallization.

Since now carboxylate MOFs are largely used as sorbents, let us consider their synthesis in more detail. There are several synthetic approaches to carboxylate MOFs, and all of them necessitate the presence of a base, as a rule, amine, for deprotonation of an organic acid (future linker) and initiation of reaction. Therewith, competitive coordination of the base and organic acid should be excluded.

The so-called "diffusion" method has been the most common until recently. A necessary condition of the synthesis is that the components are readily soluble in the reaction mixture. During synthesis, a volatile amine slowly diffuses into a dilute solution of a metal salt and an organic acid at room temperature and atmospheric pressure [39–41]. This procedure is disadvantageous by too long synthesis times (1–2 weeks). The diffusion synthesis provides coarse crystals (several hundred micrometers) which are basically used for structural studies but are unsuitable for selective separation and catalysis because of the complicated mass transfer.

An alternative, "solvothermal" procedure, allows the synthesis time to be reduced to 24 h. In this case, the crystallization of MOFs from dilute solutions in polar solvents (DMF, water, acetonitrile) is carried out in an autoclave at a moderate temperature (no higher than 110°C) [32, 42]. Conditions of the solvothermal synthesis lift reagent solubility restrictions. Mixed solvents are sometimes used to control the solution polarity, solvent–ligand exchange kinetics, and rate of product crystallization. As a rule, MOF crystals formed by the solvothermal synthesis are better candidates for technology applications. Recently an express synthetic procedure has been suggested (synthesis time 0.5–4 h) [43]. This procedure envisages direct addition of an amine at room temperature in a reaction medium containing a solution of a metal salt and an organic acid. In this case, high-purity nanocrystals are formed in high yield (~90%). The one-pot synthesis by the above three procedures is highly reproducible and readily scaled [44].

*Application of MOFs as sorbents.* As mentioned above, the chemical and steric structure of MOFs are characteristically readily controlled. Purposeful "design" at the molecular level provided materials used to success in various fields. In particular, MOFs are widely used for sorption and selective separation of gases ($N_2$, Ar, $CO_2$ [45, 46] and methane [29, 32]).

However, despite of the huge number of presently available MOFs, only few of them have been explored as hydrogen adsorpbens [5, 47, 48]. The most attractive feature of MOFs is their controllable structure–property relationship. Metal–organic frameworks possess clear geometric characteristics and are hybrid structures: They combine an organic and an inorganic components (metal ion or its oxide cluster). In this connection, there are two basic ways to enhance the physical sorption of hydrogen in MOFs: to increase the interior surface area and/or volume of pores and to increase of the energy of hydrogen binding with the metal–organic framework [49].

With this in mind, let us consider in more detail the major factors controlling hydrogen sorption in MOFs.

*Specific surface area.* As mentioned above, carboxylate MOFs which are being intensively studied as prospective hydrogen sorbents, have exceptionally large specific surface areas. In this connection a question arises how this MOF parameter affects the physical sorption of hydrogen. It was found that MOFs with high specific surface areas (above 1000 $m^2 g^{-1}$) show no direct correlation between specific surface area and hydrogen adsorption [48]. This is what distinguishes MOFs from most porous carbon materials (except for nanofibers) and zeolites in which hydrogen adsorption increases with increasing specific surface area irrespective of morphology. The lack of linear correlation between hydrogen capacity and surface area is natural for MOFs and some other microporous materials. Adsorption is actually contributed by the total pore volume, rather than formal specific surface area [12].

This statement is well illustrated by the results of research on the synthesis and adsorption characteristics

of MOF-5 (IRMOF-1). As already mentioned, MOF-5 it built by octahedral $Zn_4O$ $(O_2C–)_3$ clusters linked by linear phenylene units which form a cubic framework with pseudospherical pores. This metal–organic system was synthesized by three methods: diffusion, solvothermal, and express [16, 29, 48, 50, 51]. It was found that MOF-5 samples prepared by different procedures, have different specific surface areas, even though, according to X-ray fluorescence and diffraction data, their structures are identical. The specific surface area of the sample synthesized by Yaghi and co-workers by the solvothermal procedure (3362 $m^2 g^{-1}$) [48] is much larger than that of the sample synthesized by Panella and Hirsher by the express procedure (572 $m^2 g^{-1}$ by BET and 1014 $m^2 g^{-1}$ by Langmuir) [16]. Therewith, the hydrogen adsorption capacities of these samples are close to each other (Table 3). The sample synthesized by the express method coincides in hydrogen adsorption capacity (1.6 wt%, 77 K, 1 MPa) with the sample synthesized in solvothermal conditions (1.32 wt%, 77 K, 0.1 MPa). Apparently, this fact provides direct evidence to show that hydrogen sorption is controlled by other factors which will be considered below.

*Pore shape and size.* Metal–organic frameworks are extremely high-porosity systems but pore volume is not a unique factor responsible for their hydrogen adsorption capacity. For example, MOF-177 [$Zn_4O(btb)_2$btb = 1.3.5-tris(4-carboxyphenyl)benzene] has the largest specific surface area on record (4500 $m^2 g^{-1}$). According to X-ray diffraction data, MOF-177 has a (3, 6) coordination lattice formed by $Zn^{2+}$ oxide and a triangular carboxylate secondary structure (Fig. 4). The large pore is depicted as a sphere inscribed into the framework, and its diameter is determined by the distance between the van der Waals surfaces of framework atoms.

The calculated pore volume of this metal–organic framework is 0.69 $cm^3 cm^{-3}$. The MOF contains channels and cavities (diameter 10.9–11.8 Å) in channel crossing points (Fig. 4, Table 4) [55]. Despite of such "outstanding" geometrical characteristics, this system is inferior in hydrogen capacity than materials with smaller surface areas, such as IRMOF-8 (Table 3). Hydrogen adsorption of MOF-177 does not reach saturation at 77 K and atmospheric pressure, since in these conditions hydrogen is weaker adsorbed than nitrogen (which is used in surface measurements) and pores are not filled at low pressures. No saturation was also observed under the same conditions (77 K, 0.1 MPa) in a systematic research [48] on hydrogen adsorption of representatives of the above-mentioned series of IRMOFs (Table 3. According to calculations,

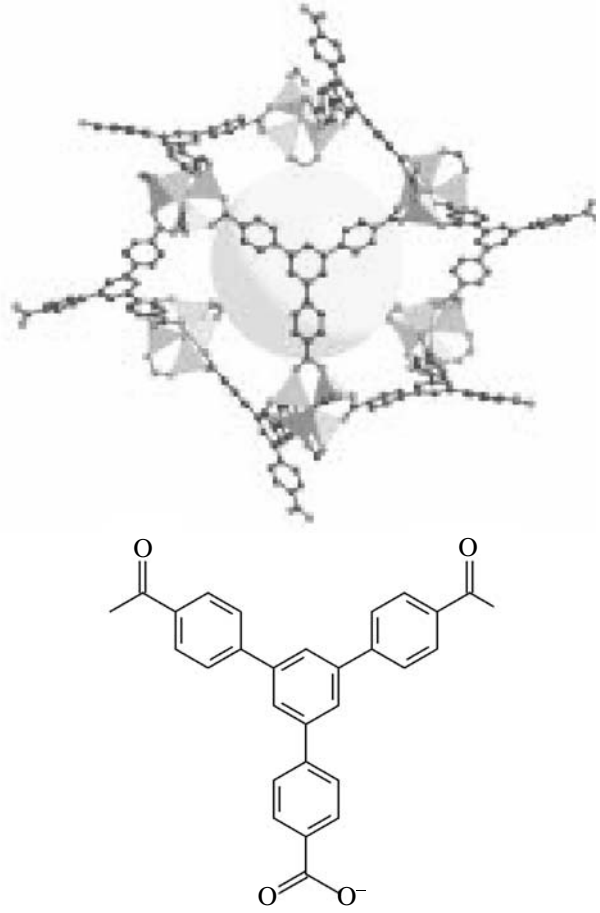


**Fig. 4.** Structure of MOF-177.

only a small fraction of the total pore volume is filled by hydrogen molecules. Consequently, for enhanced hydrogen adsorption the pore geometry should be optimized to reduce the free interior space.

What are ideal pores for effective hydrogen sorption in MOFs? An optimum material should have a large total pore volume, and the pore diameter should fit, as good as possible, the molecular diameter of the adsorbed gas. Smaller pores favor hydrogen interaction with the aromatic nuclei of the organic fragments in MOFs. This increases the energy of hydrogen binding [54]. Thus, effective sorption is favored by a great number of small pores with a diameter fitting the molecular diameter of hydrogen, rather than large pores [56]. To this end, organic or inorganic guest structures can be introduced into MOF cavities to form a secondary microporous structure and create additional centers for hydrogen adsorption.

The free space between organic fragments in most MOFs is too large for effective hydrogen sorption (Table 4). For example, the space between the phenylene planes in MOF-5 (Fig. 1) can be presented as

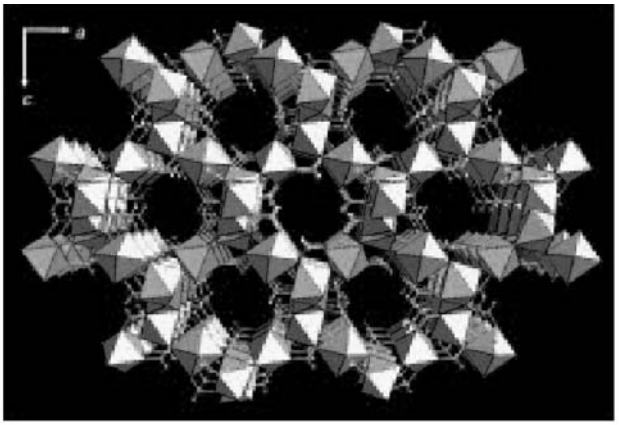

**Fig. 5.** Crystal structure of $Mn(HCO_2)_2$.

an almost spherical pore with a diameter of 12 Å which is much larger than the kinetic molecular diameter of hydrogen (2.8 Å). Thus, even at monolayer filling, some free space remains in the pore center. Pores can be reduced to an optimum size by changing their shape, for example, to spherical or elliptic [5].

The effect of pore geometry is exemplified by the high hydrogen adsorption capacity of MIL-53 obtained on the basis of $Al^{3+}$ and $Cr^{3+}$ phenylene dicarboxylates [47]. The sample on the basis of chromium had a hydrogen capacity of ~3.1 wt% and that on the basis of aluminum, ~3.8 wt% (77 K, 1.6 MPa, Table 3). However, these samples, like the MOF-5 sample synthesized by Panella and Hirsher [16], do not adsorb hydrogen at room temperature.

MIL-53 is a convenient model for comparisons with traditional carriers with close geometric characteristics, such as charcoals and zeolites. The BET specific surface area of MIL-53 of 1100 $m^2 g^{-1}$ compares with the mean specific surface area of nanocarbon materials and exceeds the respective parameter for zeolites. The MIL-53 framework is formed by one-dimensional channels 8.5 Å in diameter which compares with that of zeolite cages (6–12 Å) and is smaller than those characteristic of IRMOFs, in particular MOF-5 (12–15 Å). Therewith, the hydrogen capacity of MIL-53 is slightly higher than those of CaX zeolite (2.19 wt%, Table 2) and charcoals (2.15 wt%) [12]. Probably, of importance here is the geometry of channels, since zeolites generally have a three-dimensional system of channels, whereas MIL-53, one-dimensional channels without branches. However, additional experimental data on absorption mechanism are required for more substantiated conclusions.

An interesting object for research of the contribution of such parameters as specific surface and pore size is manganese formate $Mn(HCO_2)_2$ [46]. Its BET specific surface area (~240 $m^2 g^{-1}$) corresponds to the average value for zeolites. According to X-ray diffraction data, the structure is formed by one-dimensional channels with an internal diameter of 5.5 Å, like with MIL-53 (Fig. 5). Each octahedron in the picture represents an Mn(II) cation linked to six formate ligands. The accessible free volume of channels comprises ~33% of the total volume (Table 4). It appeared that the hydrogen adsorption capacity of $Mn(HCO_2)_2$ (0.9 wt%) is slightly higher than that of ZSM-5 zeolite (0.7 wt%, Tables 2 and 3). Note that the hydrogen capacity of manganese formate is lower by as little as ~35% than that of MOF-5, even though its specific surface area is smaller 15-fold. This effect can be attributed to the fact that the pore size in $Mn(HCO_2)_2$ fits the kinetic molecular diameter of hydrogen.

*MOFs with the catenane structure.* One of the ways to make MOF pore sizes closer to the molecular size of hydrogen, is catenane formation. Catenane structures are formed by intergrowth of two or more identical frameworks, provided an excess free pore volume is available. The so-called "catenanization" can be carried out by interlocking, when two or more identical frameworks are maximally distant one from another or by intertwining, when the distance between them is minimal and the structures come into close contact with each other [24, 27, 57]. For example, IRMOF-11 [organic fragment 4,5,9,10-tetrahydropyrene-2,7-carboxylate (hpdc), Scheme (1)] is formed by two intertwining frameworks (Fig. 3). Interpenetration of two or more systems is traditionally considered to prevent formation of high-porosity frameworks because of the reduction of pore volume. However, intertwining of two identical frameworks with a minimum substitution reduces pore diameter, ensures more favorable surface area-to-pore volume ratio, and makes the system more stable thermally [44]. These factors favor higher hydrogen adsorption capacities. Actually, intertwined IRMOF-9, IRMOF11, and IRMOF-13 (Fig. 3) show higher hydrogen adsorption capacities compared to MOF-5 (Table 3). For example, the hydrogen capacity of IRMOF-13 (Fig. 3) formed by pyrene units is almost double that of MOF-5 in spite of the fact that the latter has a larger pore volume. This effect is directly related to the reduction of pore diameter due to catenane formation.

Intertwined structures are advantageous in that they have increased total volume of pores accessible for hydrogen (Table 3). This is evident form a comparison of hydrogen adsorption of intertwined IRMOF-13 (0.89%) with normally structured IRMOF-20 whose formal surface area is 3 times as large (1.25%).

The fact that adsorption parameters are appreciably improved by the optimization of pore size due to formation of interpenetrating structures is evident from a comparison of hydrogen adsorption by the MOF-5 and [Cu(hfipbb)($H_2$hfipbb)$_{0.5}$] systems. The latter MOF comprises two interpenetrating three-dimensional metal–organic frameworks [50]. Because of the "catenane" structure, the accessible pore volume in [Cu(hfipbb)($H_2$hfipbb)0.5] is much reduced and comprises 11.6% of the total pore volume (Table 4), which is 6.6 times smaller than in MOF-5 (76.8%). But, therewith, [Cu(hfipbb)($H_2$hfipbb)$_{0.5}$] absorbs only 1.8 times less hydrogen at room temperature than MOF-5 (1.0%, 4.8 MPa, Table 3). This phenomenon is explained, in particular, by the fact that [Cu(hfipbb)·($H_2$hfipbb)$_{0.5}$] contains pores of two types: small (~$3.5 \times 3.5$ Å) and large (~$5.1 \times 5.1$ Å) which are smaller than MOF-5 pores ($7.7 \times 7.7$ Å).

An example of a MOF whose pore size fits well the molecular size of hydrogen is provided by $Cu_3(TATB)_2(H_2O)_3$ [49]. The pose size in this system is effectively reduced by two intertwining frameworks (Langmuir surface area ~3800 $m^2\,g^{-1}$, total pore volume 1.45 $cm^3\,g^{-1}$). As seen from Table 3, the hydrogen capacity of $Cu_3(TATB)_2(H_2O)_3$ is ~1.9 wt% hydrogen (10.6 mg $cm^{-3}$) at 77 K and atmospheric pressure, which is higher than the respective value for MOFs of normal structure with a large surface area : 1.35 wt% in IRMOF-20 (4346 $m^2\,g^{-1}$) and 1.25 wt% in MOF-177 (4526 $m^2\,g^{-1}$).

*Nature of organic fragment.* Organic units with highly polarized aromatic fragments, such as phenylene, naphthylene, bipyridine, and biphenylene, are widely used in the synthesis of MOFs to form a rigid framework. These molecular structural units are similar in chemical nature to carbon nanomaterials, in particular, nanotubes formed by $sp^2$-carbon atoms. An important difference between MOFs and carbon nanomaterials consists in that chemical modification of the latter does not strongly affect the energy of physical sorption [5]. At the same time, modification of the organic components of MOFs ensures stronger interaction of the framework surface with hydrogen.

The effect of chemical modification of an organic fragment with preservation of MOF topology is exemplified by the synthesis of a series of IRMOFs. It was found that the hydrogen adsorption per formular unit, both at 77 K and at room temperature, increased with increasing number of aromatic rings in the organic fragment. Thus, the length and width of the organic unit significantly affect the adsorption properties of the system (Table 3) [29, 48]. The maximum adsorption increased from 4.2 molecules of $H_2$ per formula unit in IRMOF-8 (naphthalene-2,6-dicarboxylate organic units) to 8.9 in IRMOF-11 (4,5,9,10-tetramethylphenylene-2.7-dicarboxylate). Simultaneously, the gravimetric hydrogen capacity of IRMOF-11 is almost double that of IRMOF-18 formed by 2,3,5,6-tetraphenylene-1,4-dicarboxylate fragments (Table 3). The physical hydrogen sorption was reached by using biphenylcarboxylate as the starting molecular building block (IRMOF-13, Table 3). These results show that the more aromatic are the organic linkers, the stronger hydrogen adsorbents are the MOFs. In should be noted that bulky and branched organic fragments favor much smaller pore diameters. Thus, the question of what is responsible for increased absorptivity—optimized pore size or surface energy—remains open.

Evidence for the effect of the organic fragment on hydrogen binding was obtained by inelastic neutron scattering (INS) for the series: IRMOF-1 (MOF-5), IRMOF-8, IRMOF-11, and IRMOF-177 [58]. Numerous well-defined localized hydrogen binding sites were revealed inside MOF cavities. According to the INS data, the mode of hydrogen binding varies considerably with MOF type, and, at an identical inorganic component, is influenced directly by the nature of the organic linker. These results suggest that the hydrogen adsorption capacities of MOFs can be effectively increased by the synthesis of materials with increased contents of highly polarized polyaromatic fragments to provide increased hydrogen–surface interaction energy. This approach was successfully applied for MOFs formed by polyaromatic binaphthyl compounds [$Zn_4(\mu_4\text{-}O)(L_1)_3(DMF)_2$] and [$Zn_4(\mu_4\text{-}O)(L_2)_3$] (Scheme 2) [56].

Even though the geometric characteristics, i.e. specific surface area and pore volume, of [$Zn_4(\mu_4\text{-}O)\cdot(L_1)_3(DMF)_2$] (502 $m^2\,g^{-1}$, 0.20 $m^3\,g^{-1}$) and [$Zn_4(\mu_4\text{-}O)(L_2)_3$] (396 $m^2\,g^{-1}$, 0.13 $m^3\,g^{-1}$) much worse than those of MOF-5, the hydrogen adsorption capacities of these three materials are very close to each other (Table 3). Thus, the "interpenetrating" metal–organic frameworks with polyaromatic organic fragments are better hydrogen adsorbents at room temperature. On the other hand, the hydrogen adsorption capacities of [$Zn_4(\mu_4\text{-}O)(L_1)_3(DMF)_2$] and [$Zn_4(\mu_4\text{-}O)(L_2)_3$] are very close to those of single-wall nanotubes (Tables 2 and 3). Apparently, the interpenetration of lattices enhances interaction of hydrogen molecules with MOF surface. This happens due to multiple contacts simultaneously with several aromatic nuclei of both interpenetrating frameworks, which enhances the physical sorption of hydrogen.

**Scheme 2.**

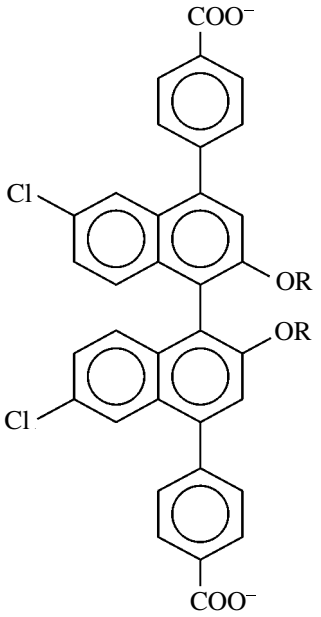


Organic fragment in $[Zn_4(\mu_4\text{-}O)(L_1)_3(DMF)_2]$ (R = ethyl) and $[Zn_4(\mu_4\text{-}O)(L_2)_3]$ (R = benzyl).

Like with node centers in nanotube "rovings," these adsorption centers in interpenetrating MOFs have increased energy of hydrogen binding.

It was found that functional substituents in the organic fragments of MOFs have no essential effect on the hydrogen adsorption capacity or even decrease it (Table 3) [44]. This fact suggests that here several oppositely directed effects are operative. On the one hand, the pore diameter in MOFs with various substituent groups decreases from 12.1 Å in IRMOF-1 to ~9.6–9.8 Å in IRMOF-2 (organic fragment 2-bromophenylenedicarboxylate), IRMOF-3 (organic fragment 2-aminophenylenedicarboxylate), and IRMOF-6 (organic fragment 1,2-dihydrocyclobutylphenylene-3,6-dicarboxylate, Table 4). Therewith, according to calculations, electron-donor groups, such as $NH_2$ or Me, can improve the interaction energy of hydrogen with the phenylene ring by ~15%. However, hydrogen adsorption capacity of IRMOF-2 is only slightly higher than that of MOF-5 (Table 3). The weak electron-acceptor effect of bromine in the phenylene ring (IRMOF-2) is compensated by its strong interaction with hydrogen, but the adsorption capacity of IRMOF-3 is lower than that of MOF-5. In the case of IRMOF-20 whose crystal lattice contains two intercrossing spherical pores (Fig. 6), the polarizability of thieno[3.2-*b*]thiophene groups essentially improves the hydrogen sorption due to stronger interaction of hydrogen with the organic fragment, but the heavy sulfur atom reduces the gravimetric capacity of the resulting system. As a result, MOF-5 and IRMOF-20 do not differ from each other in absorption capacity. As follows from the aforesaid, the above-mentioned functional groups favor effective hydrogen adsorption, but heavy substituents (Table 3) reduce the gravimetric hydrogen capacity.

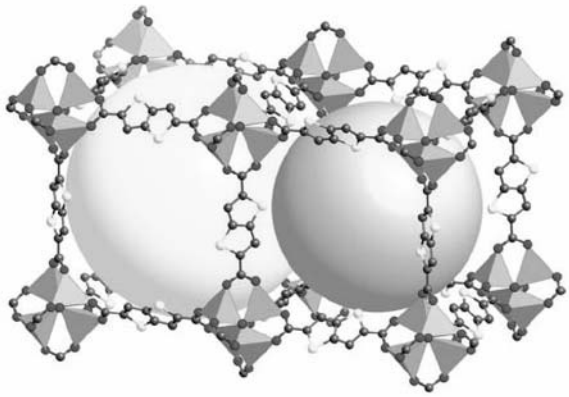

**Fig. 6.** Structure of IRMOF-20 formed by thieno[3,2-*b*]-thiophene-2,5-dicarboxylate fragments.

*Flexibility of organic fragments.* Until recently flexibility of the organic fragment in MOFs was considered to be more likely a negative feature because of the uncertain configuration of the resulting system and the probable decrease of its thermal stability. Recently flexible heterocyclic fragments became used in MOF design, along with rigid polyaromatic carboxylate units [59]. A prominent feature of such frameworks consists in the ability of their pores to contract after sorption of guest molecules and dilate after their desorption, and, therewith, the response of the porous framework depends on the nature of the guest molecule.

An example of such systems is $[Zn_2(1,4\text{-bdc})_2 \cdot (dabco)]_4$ [60]. This compound has a strong and flexible metal–organic framework which dynamically reacts on guest molecules. Its hydrogen adsorption capacity is 2.0 wt% (77 K, 0.1 MPa), which is close to the highest values of this parameter found in MOF-505 and HKUST-1 (Table 3). However, further investigations are required to reveal all advantages such systems offer for physical hydrogen sorption.

*Coordinately unsaturated (open) centers at metal ion.* As hydrogen adsorbents, MOFs are advantageous over carbon materials in that metal ions incorporated in MOFs can stronger, than carbon, bind hydrogen. Actually, hydrogen adsorption is much dependent on the inorganic component of the metal–organic framework, i.e. on the nature of the metal cation or oxide. An INS study showed that MOFs have two hydrogen

binding centers: metal ions and organic fragments [58]. Metal ions are known to play an important role in many processes, including adsorption and catalysis. The principles of MOF synthesis based on the modular chemistry make it possible to stabilize accessible coordinately unsaturated centers in a porous crystal material [53]. The basic approach to forming an open center at the metal ion consists in the following: Binuclear carboxylate clusters create the basis of an SBU, and axial positions in these clusters are occupied by labile ligands. An open coordinately unsaturated center is formed when an axial ligand is removed by evacuation, but the framework preserves porosity due to the rigidity of the structure. Coordinately unsaturated centers are very reactive, and, therefore, care must be taken to avoid formation of dimeric clustes or polymeric structures after removal of axial ligands. The function of rigid carboxylate units fixing the spatial configuration serve just to stabilize these active centers.

The contribution of such coordinately unsaturated centers (metal ions) into hydrogen adsorption capacity is quite essential [44]. This is well illustrated by the fact that MOF-505 has the highest hydrogen capacity among presently known MOFs (2.47 wt% at 77 K and 0.1 MPa, Table 3) [53]. The formula of this compound is $[Cu_2(bptc)(H_2O)](DMF)_3(H_2O)]$. The lattice nodes are occupied by square $Cu_2(O_2C)_4$ clusters. The three-dimensional structure of this MOF features two kinds of pores 8.30 and 10.10 Å in diameter (Table 4). The total accessible pore volume is 37.1%, which is smaller than in some representatives of IRMOFs on the basis of $Zn^{2+}$ (Table 4) and in isoreticular MOFs (Table 3). Probably, such an extremely high hydrogen capacity is provided by the inorganic cluster whose coordinately unsaturated center $Cu^{2+}$ has a higher hydrogen binding energy than $Zn^{2+}$. Moreover, increased hydrogen adsorption capacity is due to a small pore diameter in this MOF. In the referred work, active centers are released by removal of axial ligands, water molecules, in a vacuum.

Evidence for the assumption that coordinately unsaturated center affect the physical sorption of hydrogen was obtained from measured isosteric heats of adsorption, which give a quantitative estimate for the strength of hydrogen interaction with an active center at a metal ion [44]. The example of MOF-74 systems [on the basis of Zn(II) 2,5-dihydroxyphenylenedicarboxylates] and HKUST-1 [on the basis of Cu(II) phenylene-1,3,5-tricarboxylates] was used to characterize the contribution of the nature of the coordinately unsaturated center. These two frameworks surpass in the gravimetric capacity other representatives of the IRMOF series (Table 3). The isosteric heats of adsorption of HKUST-1 and MOF-5 suggest a stronger interaction of the $H_2$ molecule with the $Cu_2(O_2C–)$ than with $Zn_4O(O_2C–)_6$. Under low-loading conditions, the isosteric heats of adsorption of HKUST-1 is higher by 2.0 kJ $mol^{-1}$ compared to MOF-5. Actually, the hydrogen capacity of HKUST-1 is almost double that of MOF-5 (Table 3) and slightly higher than that of MOF-505 which, too, contains coordinately unsaturated $Cu^{2+}$ centers (Table 3 [53]).

Thus, the low-pressure hydrogen capacity can be effectively increased due to stabilization of coordinately unsaturated centers in MOFs and selection of more effective, than $Zn^{2+}$, metal ions.

Comparing the effects of the "organic" and "inorganic" factors on hydrogen capacity one can conclude that the organic fragment still contributes much less into hydrogen adsorption than inorganic. Recent experimental works gave evidence to show that inorganic clusters on the basis of metal ions are more effective centers of hydrogen binding and favor physical hydrogen sorption.

## HYDROGEN SPILLOVER

One of the most perspective ways for increasing hydrogen absorption capacity is presently provided by secondary hydrogen spillover [61–63].

Spillover is defined as migration of an active species absorbed on one center to a neighboring center which itself does not adsorb such species in usual conditions [62, 64]. As a result, centers located in the immediate vicinity of the primary adsorption center become accessible for adsorption. The catalytic center (metal) ensures dissociation of hydrogen molecules into atoms, and the atomic hydrogen spills over surface to a receptor. As a rule, a mechanical mixture of a catalyst (source of atomic hydrogen) with a receptor is used; receptors are most commonly inert or have a low adsorption capacity [65, 66]. In some cases, physical "bridges" are required to provide hydrogen spillover from the dissociation center to receptor [67]. Such bridges are extremely important because of the existence of an energy barrier to the surface diffusion of hydrogen from the catalytic center to receptor. At present, carbon bridges formed by surface carbonization are applied [62]. If the source of atomic hydrogen is a metal particle of a low-capacity carrier, the total adsorption capacity can be increased by addition of a high-capacity receptor. In this case, migration of atomic hydrogen from the metal particle to carrier is a primary spillover and transfer to the receptor is a secondary spillover (Fig. 7). Thus, secondary hyd-

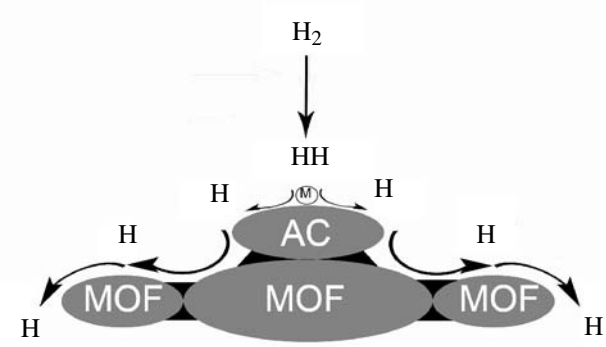


**Fig. 7.** Spillover of atomic hydrogen from metal to activated carbon carrier (primary receptor) and to MOF (secondary receptor).

rogen spillover consists in the dissociative chemisorption of hydrogen on a metal catalyst with the subsequent migration of atomic hydrogen to the surface of a carrier contacting the metal (primary hydrogen receptor) and then to the second carrier (secondary receptor). Carbon bridges (black fields in Fig. 7) promote spillover.

In case of single-wall nanotubes ($S_{sp}$. 820 $m^2 g^{-1}$, pore diameter 12 Å) and superactivated charcoal AX-21 ($S_{sp}$ 2880 $m^2 g^{-1}$), the hydrogen adsorption capacity was essentially increased by addition of a Pd/C catalyst (5 wt%) with simultaneous introduction of carbon bridges. As mentioned above, the role of the catalyst is to promote the dissociation of hydrogen molecules into atoms, thus facilitating diffusion into the space between graphene layers or into interior nanotube cavities [62].

Carbon bridges are formed by addition of a carbon precursor (D-glucose) to a mechanical mixture of components (receptor : precursor : source ratio 8 : 1 : 1) with the subsequent heat treatment at 673 K. In the presence of such carbon bridges, the hydrogen capacity at room temperature increases 2–3 times both with superactivated charcoal and with nanotubes and both at low (100 kPa) and at high (10 MPa) hydrogen pressures. In these conditions, superactivated charcoal AX-21 (Table 5) showed a higher hydrogen adsorption capacity than single-wall nanotubes.

The adsorption capacities of multiwall nanotubes (MWNTs) were improved due to hydrogen spillover and by their microwave treatment by hydrogen plasma for forming defects on tube walls, which, too, facilitates access of hydrogen to the interior surface between graphene layers (Table 5) [68]. So, if the hydrogen capacity of defectless MWNTs was 0.6 wt% (298 K, 10.7 MPa), then after plasma treatment it more than doubled (to 1.4 wt%). Subsequent introduction of Pd increased the hydrogen adsorption capacity to 4.5 wt% that is one of the best values for today.

Spillover proved to be quite an effective way to increase the adsorption capacity of carbon nanofibers (CNFs). For example, addition of 2 wt% of Pd

**Table 5.** Spillover effect on hydrogen adsorption

| Material | Specific surface area (BET), $m^2 g^{-1}$ | $H_2$ adsorption, wt % | Conditions | Reference |
|---|---|---|---|---|
| CNF + 2%Pd | | 1.38 | 293 K, 7.7 MPa | [11] |
| SWNTs/5%Pd/C/carbon bridges 8 : 1 : 1 | 820 | 0.038 | 298 K, 100 kPa | [62] |
| AX-21/5%Pd/C/carbon bridges 8 : 1 : 1 | 2880 | 0.04 | 298 K, 100 kPa | [62] |
| AX-21/5%/Pd/C/carbon bridges 8 : 1 : 1 | 2880 | 1.8 | 25°C, 10 MPa | [62] |
| MWNTs | | 0.6 | 25°C, 10.73 MPa | [69] |
| MWNTs/20%Pd/plasma treatment | | 4.5 | 25°C, 10.72 MPa | [69] |
| $Zn_4O(bdc)_3$ + 5%Pt/C/carbon bridges, IRMOF-1, MOF-5 | 3362 | 3.0 | 25°C, 10 MPa | [63] |
| $Zn_4O(ndc)_3$ + 5%Pt/C/carbon bridges, IRMOF-8 | 1466 | 4.0 | 25°C, 10 MPa | [63] |

increased the hydrogen adsorption capacity of CNFs at room temperature (Table 5) [11].

Recently secondary hydrogen spillover was also revealed in MOFs [63]. It was found that these systems adsorb much more hydrogen when mechanically mixed with a supported catalyst (Fig. 7). Thus the adsorption capacity of IRMOF-8 in the presence of 5% Pt/C increased up to 4% at 298 K and 10 MPa (Table 5), which is higher by a factor of 8 than the adsorption capacity of IRMOF-8 in the same conditions (0.5%, Table 3). The adsorption capacity of MOF-5 reached 3% (298 K, 10 MPa) owing to this effect. In these conditions, the physical sorption of hydrogen is completely reversible. In the given example, charcoal is a primary hydrogen receptor and IRMOF-1 (MOF-5) and IRMOF-8, secondary. For optimum effect, carbon bridges were introduced into the system. To form such bridges, a three-component mechanical mixture containing a MOF, catalyst, and cellulose was prepared and then subjected to the carbonization procedure similar to that described above for carbon carriers. The calculated quantity of absorbed hydrogen is ~34 hydrogen atoms per $Zn_4O(C_{12}H_6O_4)_3$ formula unit. Hence, the theoretical hydrogen sorption maximum is ~6.5% (298 K, 10 MPa), that is already close to real demands of motor industry.

As seen from the aforesaid, at present MOFs have lower hydrogen adsorption capacities than carbon nanomaterials (Tables 1 and 3). However, in the presence of platinum group metals and hydrogen spillover, the hydrogen adsorption capacities of MOFs and carbon materials become practically identical. This can be explained by the prevailing role of the catalyst: a supported platinum group metal with a high hydrogen affinity. In this case, the features of the sorbent (hydrogen receptor) are leveled down.

## CONCLUSION

Metal–organic frameworks have some common properties, such as large specific surface area and high porosity (open channels), with zeolites and contemporary carbon materials and contain hydrogen binding centers–metal ions. In physical characteristics and structure, MOFs and single-wall carbon nanotubes, too, are close to each other: These are systems with a low density, they characteristically contain open channels and cavities, and most MOFs include aromatic carbon in their chemical structure. As hydrogen sorbents, MOFs are advantageous over carbon materials in some respects: Their channels are absolutely ordered, which provides more effective hydrogen access to their interior space, and the surface inside MOF channels can be easily modified to change their curvature, which allows optimization of sorption properties. MOFs are prepared by a facile reproducible synthesis, whereas economic large-scale production of nanotubes is presently impractical [69]. Activation of MOFs does not require severe conditions, unlike nanotubes (nitric acid, $CO_2$, 700°C), or template annealing, unlike zeolites. As a rule, exposure of MOFs to a vacuum at 25–190°C is sufficient to free their channels and cavities from solvent or excess initial reagent.

Analysis of published data shows that in hydrogen absorption capacity MOFs rank between nanocarbon materials and zeolites. Actually, the hydrogen absorption capacities of metal–organic frameworks sometimes called organic zeolites are close or even higher than those of zeolites (Tables 2 and 3). Even though MOFs are presently inferior to nanocarbon materials inferior in hydrogen adsorption capacity (Tables 1 and 3), the structural diversity of MOFs gives an occasion for optimism. Zeolites and carbon materials have a limited number of structural parameters which can be varied to increase the hydrogen absorption capacity. With zeolites, one can introduce extra-framework cations which are the additional centers of hydrogen binding and increase the surface area. However, these parameters can be varied to a certain limit. With carbon nanomaterials, such a variable parameter is surface area which is linearly related to hydrogen adsorption capacity, but this parameter cannot be increased over a theoretical limit. Theoretical simulation of hydrogen interaction with a wide range of carbon nanotubes prepared in different ways and having different geometric characteristics showed that their hydrogen adsorption limit is some wt %. The properties of MOFs can de varied almost infinitely due to variation of pore volume and diameter and polarizability of organic fragment, selection of inorganic secondary structural units, stabilization of great number of coordinately unsaturated centers in the metal–organic framework, change of topology, etc. These opportunities give grounds to expect positive dynamics in the improvement of physical hydrogen sorption parameters in crystalline microporous metal–organic frameworks.

## REFERENCES

1. Dillon, A.C. and Heben, M., *J. Appl. Phys. A,* 2001, vol. 72, p. 133.
2. Ning, G.Q., Wei, F., Lu°, G.H., Wang, Q.X., Wu, Y.L, and Yu, H., *Ibid.,* 2004, vol. 78, p. 955.
3. Zuttel, A., *Naturwissenschaften,* 2004, vol. 91, p. 157.
4. Poirier, E., Chaine, R., Bernard, P., Cossement, D.,

Lafi, L., Melanson, E., Bose, T. K., and Desilets, S., *Appl. Phys. A,* 2004, vol. 78, p. 961.

5. Rowsell, J.L.C. and Yaghi, O.M., *Angew. Chem. Int. Ed.,* 2005, vol. 44, no. 30, p. 4670.
6. Ross, D.K., *Vacuum,* 2006, vol. 80, no. 10, p. 1084.
7. Tibbets, G.G., Meisner, G.P., and Olk, C.H., *Carbon,* 2001, vol. 39, p. 2291.
8. Badzian, A., Badzian, T., Breval, E., and Piotrowski, A., *Thin Solid Films,* 2001, vols. 398–399, p. 170.
9. Kiyobayashi, T., Takeshita, H.T., Tanaka, H., et al., *J. Alloys Comp.,* 2002, vols. 330–332, p. 666.
10. Heine, T., Zhechkov, L., and Seifert, G., *Phys. Chem. Chem. Phys.,* 2004, no. 6, p. 980.
11. Marella, M. and Tomaselli, M., *Carbon,* 2006, vol. 44, p. 1404.
12. Nijkamp, M.G., Raayamakers, J.E.M.J., Dillen, A.J., and Jong, K.P., *Appl. Phys. A,* 2001, vol. 72, p. 619.
13. Bernard, P. and Chachine, R., *Langmuir,* 2001, vol. 17, p. 1950.
14. Patrick, J.W., Arenillas, A., Shi, W., and Snape, C.E., *Carbon,* 2006, vol, 44, p. 1376.
15. Rawat, D.C., Talapatra, S., Lafdi, K., and Migone, A.D., *Appl. Phys. A,* 2004, vol. 78, p. 969.
16. Panella, B. and Hirsher M.J., *J. Alloys Comp.,* 2005, vols. 404–406, p. 399.
17. Hirscher, M., Becher, M., Haluska, M., et al., *Ibid.,* 2002, vols. 330–332, p. 654.
18. Ritschel, M., Uhlemann, M., Gutfleisch, O., et al., *Appl. Phys. Lett.,* 2002, vol. 80, p. 2985.
19. Weitkamp, J., Fritz, M., and Ernst, S., *Int. J. Hydrogen,* 1995, vol. 20, p. 967.
20. Schlapbach L., Zuttel A., *Nature,* 2001, vol. 414, p. 353.
21. Langmi, H.W., Walton, A., Al-Mamouri, M.M., et al., *J. Alloys Compounds,* 2003, vols. 356–357, p. 710.
22. Langmi, H.W., Book, D., Johnson, S.R., et al., *Ibid.,* 2005, vols. 404–406, p. 637.
23. Scarano, D., Bordiga, S., Lamberti, C., et al., *Applied Catalysis A: General,* 2006, vol. 307, no. 1, p. 3.
24. Rowsell, J.L.C. and Yaghi, O.M., *Microp. Mesopor. Mater.,* 2004, vol. 73, p. 3.
25. James, S.L., *Chem. Soc. Rev.,* 2003, vol. 32, p. 276.
26. Papaefstathiou, G.S. and MacGillivray, L.R., *Coord. Chem. Rev.,* 2003, vol. 246, p. 169.
27. Rosi, N.L., Eddaoudi, M., Kim, J., O'Keefi, M., and Yaghi, O.M., *Cryst. Eng. Comm.,* 2002, vol. 68, no. 4, p. 401.
28. Yaghi, O.M., O'Keefi, M., Ockwig, N.W., Eddaoudi, M., and Kim, J., *Nature,* 2003, vol. 423, p. 705.
29. Eddaoudi, M., Kim, J., Rosi, N.L., et al., *Science,* 2002, vol. 295, p. 469.
30. Kesanli, B. and Lin, W., *Coord. Chem. Rev.,* 2003, vol. 246, p. 305.
31. Hagrman, P.J, Hagrman, D., and Zubieta J., *Angew. Chem. Int. Ed.,* 1999, vol. 38, no. 18, p. 2638.
32. Fletcher, A.J., Thomas, K. and M., Rosseinsky, M.J., *J. Solid State Chem.,* 2005, vol. 178, p. 2491.
33. Noro, S.-I., Kitagawa, S., Kondo, M., and Seki, K., *Angew. Chem. Int. Ed.,* 2000, vol. 39, no. 12, p. 2081.
34. Paz, F.A. and Klinowski, J., *Inorg. Chem.,* 2004, vol. 43, p. 3882.
35. Cao, R., Shi, Q., Sun, D., Hong, M., Bi, W., and Zhao, Y., *Ibid.,* 2002, vol. 41, p. 6161.
36. Eddaoudi, M., Li, H., Yaghi, O.M., *J. Am. Chem. Soc.,* 2000, vol. 122, 7, p. 1391.
37. Serre, C., Millange, F., Thouvenot, C., et al., *Ibid.,* 2002, vol. 124, 45, p. 13519.
38. Fenelonov, V.B., *Porous Carbon,* Novosibirsk, 1995, p. 513.
39. Yaghi, O.M., Davis, C.E., Li, G., and Li, H., *J. Am. Chem. Soc.,* 1997, vol. 119, 12, p. 2861.
40. Li, H., Davis, C.E., Groy, T.L., Kelley, D.G., and Yaghi, O.M., *Ibid.,* 1998, vol. 120, 9, p. 2186.
41. Li, H., Eddaoudi, M., Groy, T.L., and Yaghi, O.M., *Ibid.,* 1998, vol. 120, 33, p. 8571.
42. Li, H., Eddaoudi, M., O'Keefi, M., and Yaghi, O.M., *Nature,* 1999, vol. 402, p. 276.
43. Huang, L., Wang, H., Chen, J., et al., *Microp. Mesopor. Mater.,* 2003, vol. 58, p. 105.
44. Rowsell, J.L.C. and Yaghi, O.M., *J. Am. Chem. Soc.,* 2006, vol. 128, no. 4, p. 1304.
45. Skoulidas, A.I., *Ibid.,* 2004, vol. 126, no. 5, p. 1356.
46. Dubtsev, D., Chun, H., Yoon, S.H., Kim, D., and Kim, K., *Ibid.,* 2004, vol. 126, no. 1, p. 32.
47. Ferey, G., Latroche, M., Serre, C., et al., *Chem. Commun.,* 2003, vol. 24, p. 2976.
48. Rowsell, J.L.C., Millward, A.R., Park, K.S., and Yaghi, O.M., *J. Am. Chem. Soc.,* 2004, vol. 126, no. 18, p. 5666.
49. Sun, D., Ma, S., Ke, Y., Kollins, D.J., and Zhou H.-C., *Ibid.,* 2006, vol. 128, p. 3896.
50. Pan, L., Sander, M.B., Huang, X., et al., *Ibid.,* 2004, vol. 126, no. 5, p. 1308.
51. Rosi, N.L., Eckert, J., Eddaoudhi, M., et al., *Science,* 2003, vol. 300, p. 1127.
52. Dybtsev, D.N., Chun, H., and Kim, K., *Angew. Chem. Int. Ed.,* 2004, vol. 43, no. 38, p. 5033.
53. Chen, B., Ockwig, N.W., Millward, A.R., et al., *Angew. Chem. Int. Ed.,* 2005, vol. 44, no. 30, p. 4745.

54. Kesanli, B., Cui, Y., Smith, M.R., et al., *Angew. Chem., Int. Ed.,* 2005, vol. 44, no. 1, p. 72.
55. Chae, H.K., Siberio-Perez, D.Y., Kim, J., et al., *Nature,* 2004, vol. 427, p. 523.
56. Chun, H., Dubtsev, D.N., Kim, H., and Kim, K., *Chem. Eur. J.,* 2005, vol. 11, p. 3521.
57. Batten, S.R. and Robsom, R., *Angew. Chem. Int. Ed.,* 1998, vol. 37, p. 1460.
58. Rowsell, J., Eckert, J., and Yaghi, O., *J. Am. Chem. Soc.,* 2005, vol. 127, no. 42, p. 14904.
59. Shimizu, G.H., *J. Solid State Chem.,* 2005, vol. 178, p. 2519.
60. Chen, B., Eddaoudi, M., Reineke, T.M., et al., *J. Am. Chem. Soc.,* 2000, vol. 122, no. 6, p. 1159.
61. Yang, F.H. and Yang, R.T., *Carbon,* 2002, vol. 40, p. 437.
62. Lachawiec, A.J., Qi, G.S., and Yang, R.T., *Langmuir,* 2005, vol. 21, p. 11418.
63. Li, Y. and Yang, R.T., *J. Am. Chem. Soc.,* 2006, vol. 128, p. 8136.
64. Conner, W.C., Jr. and Falconer J.L., *Chem. Rev.,* 1995, vol. 95, p. 759.
65. Srinvas, S.T. and Rao, P.K., *J. Catal.,* 1994, vol. 148, p. 470.
66. Lueking, A.D. and Yang, R.T., *Appl. Catal. A,* 2004, vol. 265, p. 259.
67. Levy, R.B. and Boudart, M., *J. Catal.,* 1974, vol. 32, p. 304.
68. Mu, S., Tang, H., Qian, S., Pan, M., and Yuan, R., *Carbon,* 2006, vol. 44, p. 762.
69. Dickie, D., Shatte, G.M., Jennings, C.F., et al., *Inorg. Chem.,* 2006, vol. 45, p. 1646.

*Vera Il'inichna Isaeva,* Cand. Sc. (Chem.), Researcher, Laboratory of Catalytic Hydrogenation, Zelinskii Institute of Organic Chemistry, Russian Academy of Sciences (IOC RAS). Scientific areas of focus: metal complex catalysis, catalytic hydrogenation, heterogeneous catalysts.

*Leonid Modestovich Kustov,* Dr. Sc. (Chem.), Professor, Head of Laboratory of Development and Research of Multifunctional Catalysts, IOC RAS, Head of Laboratory of Ecological Chemistry, Chemical Department, Lomonosov Moscow State University. Scientific areas of focus: catalysis, nanomaterials, hydrogen storage, zeolites.